# Polarization dynamics in vertical-cavity surface emitting lasers

Thorsten Ackemann, Markus Sondermann

*Institut für Angewandte Physik, Westfälische Wilhelms–Universität Münster,*

*Corrensstr. 2/4, D–48149 Münster, Germany.*

*e-mail: t.ackemann@uni-muenster.de, sondema@uni-muenster.de*

**Abstract**

Experiments and their interpretation on polarization dynamics and polarization switching in vertical-cavity surface-emitting lasers operated in the fundamental transverse mode regime are reviewed. Important observations are switching events to a mode with the lower unsaturated gain and the existence of elliptically polarized dynamical transition states after the destabilization of the low-frequency polarization mode. The observations demonstrate the need to consider explicitly the phase properties of the optical field as well as nonlinear effects affecting polarization selection above threshold. Good qualitative agreement is found with a model which takes into account the spin degrees of freedom of the light field as well as of the carriers ('spin-flip model'), if the spin-flip rate is taken to be some tens of $10^9$ s$^{-1}$. This constitutes a strong – though indirect – indication that spin dependent processes are important in polarization selection in the devices investigated.

# 1 INTRODUCTION

*Vertical-cavity surface-emitting lasers* (VCSELs) are a relatively new type of semiconductor laser diodes, in which – in contrast to edge-emitting lasers – the axis of the laser emission is orthogonal to the plane of the active medium (parallel to the epitaxial growth direction). The active zone usually consists of a small number of quantum wells. These are surrounded by spacer layers which are typically only a half a wavelength thick and the cavity is closed by high-reflectivity ($R \gtrsim 0.995$) Bragg-reflectors. Reviews of technical aspects of VCSELs can be found in [1–3].

Due to the short cavity length, VCSELs operate in a single-longitudinal mode without any further measures. The active zone and thus approximately also the emitted beam can be processed to be circular. This facilitates fiber coupling tremendously in comparison to the use of edge-emitting devices. Hence VCSELs are the dominant type of laser in short-haul fiber communication networks, e.g. local-area-networks. Further applications in single-mode data transmission [4], long-haul communication systems with long-wavelength lasers [3], spectroscopy [5,6], sensor applications [6] and optical data storage [7] are intensively studied for low-power and medium-power devices. High-power devices are considered for material treatment, laser pumping, free space communication and medical applications, e.g. [8].

However, the circular symmetry of VCSEL devices is not only advantageous, but also a source of pronounced instabilities, since the *polarization* state is no longer fixed by geometrical constraints as in edge-emitting lasers. Even if most authors report a rather strong pinning of the direction of the polarization to the crystal axis in real devices [9–12] and a linearly polarized emission at threshold, the polarization degrees of freedom degrade the noise properties of the device [13–15] and may cause an intriguing spontaneous flip to the orthogonal linear polarization if the current is increased (*polarization switching (PS)*, [10,11,14,16–18]). These phenomena are obviously annoying in most of the applications mentioned above, since they are – at least to some, often large extent – polarization-sensitive. This motivates a thorough understanding of the mechanisms underlying polarization instabilities – notably PS – in VCSELs as a first step to develop control techniques.

2

It is rather well established by now, that one of the important ingredients influencing the polarization state of VCSELs are *linear anisotropies* stemming from the fact that real-world devices have no ideal rotational symmetry. There are *amplitude* and *phase* anisotropies, i.e. *dichroism* and *birefringence.* These are induced by unavoidable mechanical stress via the elasto-optic effect [12, 16] and by the electro-optic effect [19]. The birefringence leads to a removal of the frequency degeneracy of modes with different polarization and thus to a frequency splitting. Due to the dichroism these modes experience a different net gain (net gain = unsaturated gain - unsaturated losses), which leads to a selection of one polarization mode at threshold [16].

Some authors found that also the polarization selection *above* threshold is determined by the linear anisotropies [11, 14, 16, 18]. These might change due to thermal effects, which are inevitable during cw-operation due to ohmic heating. The first treatment considered the change of the gain anisotropy, if the frequency split polarization modes are thermally shifted across the gain line [16]. Further proposals have been made in [20] and [21], taking into account also frequency dependent losses or strain effects in the quantum well active region, respectively. Common to all these models is that they explain PS by a current dependent change of the *linear, i.e. unsaturated, net gain anisotropy* that becomes zero and changes its sign at the point of the PS.

A different approach is based on the nonlinear dynamics induced by the coupling of inversion populations with opposite spin and by phase-amplitude coupling. The corresponding model by San Miguel et al. is referred to as *spin-flip-model* or SFM [22, 23] (an excellent review can be found in [24]). We mention that phase-amplitude coupling is particularly strong in semiconductor lasers due to the asymmetric gain curve and often described by the so-called linewidth enhancement or $\alpha$-factor [25]. In the SFM, PS occurs due to a phase instability, i.e. a change of the phase relationship of the left- and right-handed circular polarized components of the emitted light. An important prediction of this model is that PS from the *mode favored by the net gain to the gain disfavored mode* is possible.

The situation is even more complicated because it was found in a series of careful measurements [14, 26] that the steady state polarization selection in many devices was apparently determined by the linear anisotropies (and the PS due to a change of linear dichroism) – though the decisive mechanism remained unclear (see, e.g., Sec. XI of [14]) – but that dynamical features present in details of optical spectra and transient measurements of the PS were in agreement with predictions of the SFM. Furthermore, spatial-hole burning might contribute to all situations [27, 28].

Hence, the question is how to differentiate among the proposed mechanisms from an experimental point of view. One approach is to operate the laser with current pulses with a duration far below the thermal relaxation times. A PS from the mode with higher to the mode with lower optical frequency (HF- to LF-mode, often referred to as 'type I PS', [20]) under pulsed operation has been observed in [17] and in [29]. However, it was argued that this does not give conclusive evidence for a non-thermal switching, since the plasma temperature might change even if the lattice temperature remains constant [30].

Another possibility is to look for 'fingerprints' of the nonlinear dynamics. The SFM predicts for the PS from the LF-mode to the HF-mode ('type II PS' in the terminology of [20]) the occurrence of elliptically polarized dynamical states at the PS, which lead to a reduction

3
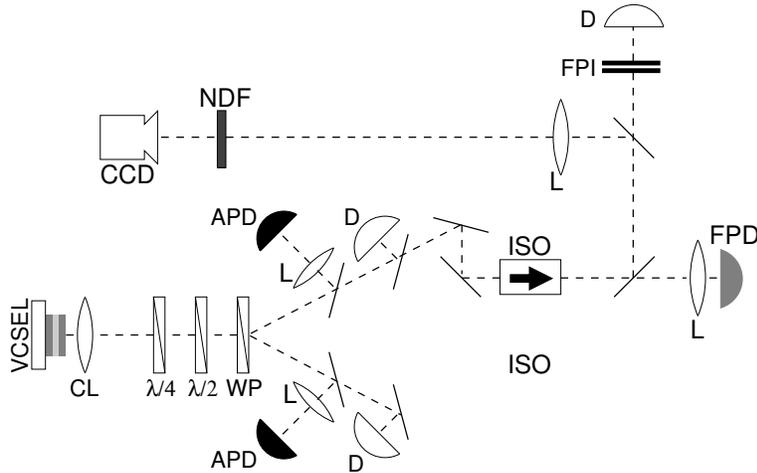
Figure 1: Scheme of the setup that was used for the experiments on the polarization dynamics of VCSELs. The abbreviations in the figure denote the different elements of the setup as follows: CL, collimation lens; $\lambda/4$, quarter-wave plate; $\lambda/2$, half-wave plate; WP, Wollaston prism; L, lenses; APD, avalanche photo-diode (1.8 GHz bandwidth); D, low-bandwidth detector; ISO, optical isolator; FPD, fast photo detectors of different types (10 GHz and 26 GHz bandwidth, respectively); FPI, scanning Fabry-Perot interferometer; NDF, neutral density filters; CCD, charge-coupled device camera. Mirrors are denoted by thick solid lines. The beam path is indicated by a dashed line. Further explanations are given in the text.

of the fractional polarization and appear as sidebands in the optical spectrum. Within the framework of the above model, characteristic spectra or similar phenomena are not predicted for type I PS. One therefore has to look for other manifestations of the switching to a mode with lower net gain. We will find it in the fact that a switching event to the gain disfavored mode is accompanied by a decrease of the output power of the laser at the point of PS.

The paper is organized as follows: In the next section we will discuss the experimental setup. Then, we will present experimental results on polarization dynamics and polarization switching of type 1 as well as of type 2. In Sect. 4, we will compare these findings with theoretical predictions by the SFM. The focus will be on our own results but we will try to put them in context with the findings of other groups. Finally, a brief outlook is given.

# 2 EXPERIMENTAL SETUP

The experiments have been performed on commercial gain-guided VCSELs (Emcore Corp., Model 8085-2010) operating in the wavelength region around 840-850 nm. We have chosen devices with an 8 $\mu$m wide aperture which are specified as single-mode devices. Their threshold currents vary between 3 mA and 5 mA (depending on device and operating temperature). Higher order transverse modes usually start to oscillate at current levels about two times the fundamental mode threshold. We want to concentrate here on the behavior within the fundamental mode regime, because the dynamics is very complex and difficult to analyze, otherwise.

A schematic version of the setup used to conduct the experiments on the polarization dynamics of VCSELs is displayed in Fig. 1. The VCSELs have been mounted in a temperature controlled copper holder. The substrate temperature of the VCSELs can be changed and stabilized in a range from 6°C to 70°C. The light emitted from the VCSEL has been collimated using an aspheric antireflection coated lens. After passing through a half-wave plate, the orthogonal polarized components of the VCSEL output are split by a Wollaston prism. For projection onto circular polarized polarization states a quarter wave plate is inserted in the beam path in front of the half wave plate. All polarization optics have been slightly misaligned in order to prevent feedback into the laser. The combination of the three elements allows the determination of the Stokes parameters, which characterize the polarization state of the emitted light completely. For each polarization component, the time averaged output power and the temporal dynamics can be measured by a low-bandwidth detector and an avalanche photo diode (APD) of 1.8 GHz bandwidth, respectively. The output of the avalanche photo diode is recorded with a digital oscilloscope with 1 GHz analog bandwidth (on the 5 mV/div scale). Radio-frequency (RF) power-spectra are measured with a PIN-diode of 10 GHz or 26 GHz bandwidth and an electrical power spectrum analyzer of 20 GHz bandwidth. In some measurements, time series obtained from the 26 GHz diode were directly monitored with a fast digital oscilloscope (LeCroy Wavemaster) with 6 GHz analogue bandwidth and a sampling rate of 20 Gs/s. Due to the low sensitivity of the photodiode, the signal had to be amplified before by 40 dB using two amplifiers (Agilent A83006A, 0.01-26.5 GHz) at the expense of losing the DC-information.

A scanning Fabry-Perot interferometer (FPI) with a finesse better than 150 and a free spectral range of 46 GHz allows for a measurement of optical spectra. Unintended back reflections into the laser are prevented by an optical isolator with more than 60 dB suppression. The near field intensity distribution of the lasers was imaged on a charge-coupled devices (CCD) camera. In experiments described here, this was used only – in conjunction with the FPI – to ensure that no high order transverse modes were excited in the current region investigated.

It turns out that in all experiments on polarization properties of VCSELs great care needs to be taken in the mechanical mounting of the devices, since the linear anisotropies – and hence the polarization properties – of VCSEL structures depend on mechanical stress (e.g., [21, 31, 32]). On the other hand, this sensitivity opens the opportunity to control them. Since this possibility will be of importance later, a brief review of the method of applying mechanical stress to VCSELs with the intention of modifying the linear anisotropies is given here.

The elastic and elasto-optic properties of a solid can be described by appropriate tensors. Hence, the magnitude and the principal axes of the birefringence can be changed by applying external stress [12, 31]. The latter will determine also the orientation of the principal axis of the cavity eigenmodes [12, 31]. Application of stress changes also the linear dichroism which is acting on the two polarization modes of a VCSEL [33], though the principal axis of the latter one was found to be always oriented roughly along the wafer axes for different devices and operating conditions [33]. The orientation of the principal axes of the birefringence does not need to be parallel to the orientation of the dichroism. In that case, one has to consider a 'projected dichroism', i.e. the dichroism that acts in the direction of the mayor axis of the cavity mode [14, 33].

The relative alignment of the anisotropies also influences the state of polarization (SOP) of the lasing device [33–35]. As proven experimentally in [33], the SOP becomes elliptical if birefringence and dichroism are misaligned. It was shown theoretically in [35] that modes with a finite ellipticity are the only stable modes in this case. The ellipticity of the SOP is measured in terms of the ellipticity angle $\chi$. This angle is given by the arc tangent of the ratio of the principal axes of the polarization ellipse. The second angle that characterizes the SOP is the orientation $\phi$, which is a measure for the tilting of the long axis of the polarization ellipse with respect to some reference direction. As stated above, this axis coincides with the orientation of the birefringence.

From the above considerations, it is expected that the VCSEL emission should be always slightly elliptical due the random nature of the direction of stress due to contacting, bonding and packaging. Indeed, it was reported in [33] that all of the investigated VCSELs had a SOP with a small but finite residual ellipticity angle. In [14] the investigated VCSELs had an ellipticity angle of '1° or less' except for the ones with a very small birefringence (in that case it was 5-10°). The apparent tendency of real VCSELs to emit in a 'more or less linear' polarization state oriented roughly along the wafer axis can be explained by the rather strong anisotropy of the tensors which relate external forces to internal strain and then internal strain to a change in birefringence [12, 31]. In our setup, the 'background' contribution to the ellipticity due to imperfections in the polarization analyzing optics is about 0.6°. On that level, we will call a VCSEL to be 'linearly polarized'.

To summarize the above findings, the magnitude and orientation of the birefringence, the dichroism and the ellipticity can be manipulated by applying stress to the VCSEL. Several methods have been proposed to achieve this purpose [21, 36]. The mount used follows the design introduced in [21], where the back plate of the TO-46 package of the VCSEL is bend over a needle providing a tensile stress on package and wafer [37]. This method is sufficient to change the anisotropies to the order of magnitude that is desired, though the stress relaxes on time scales of several hours. It is also very difficult to match exactly the same stress conditions in repetitive runs of the experiment. Hence, the measurements cannot be as complete as for devices which exhibit the desired anisotropies without application of additional stress.

Therefore, in most experiments (including all with involve a temperature scan) a rather massive and rigid submount was used to hold the VCSEL package in a smoothly fitting bore. This holder was designed in order to alter the 'intrinsic' anisotropies (i.e., the ones caused by the device contacting and packaging) as little as possible. In this mount the linear anisotropies did not change between runs except for small fluctuations (see also [14], Sect. VI). On long time scales (over years) we saw strong changes in some cases which are attributed to aging.

For a measurement of the anisotropies two different methods have been established [14], which both rely on the fact that the anisotropies determine the temporal evolution of a perturbation with orthogonal polarization to the lasing mode [14, 38–41]. Note that this definition applies also above threshold. Then 'effective' anisotropies are obtained, which are the sum of the linear (the values at threshold) and nonlinear contributions (see also [14]).

Since a perturbation to the lasing mode, which is driven by spontaneous emission noise, appears as the non-lasing mode in the optical spectrum, one possibility of measuring the
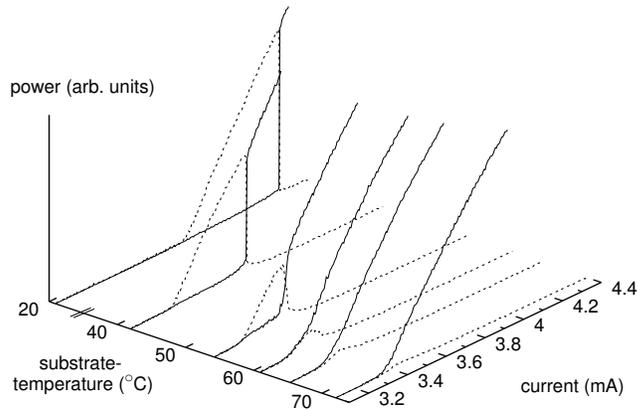
Figure 2: Polarization resolved power against current (LI-curve) in dependence of the substrate-temperature. Here – and in the following figures – solid (dashed) lines denote the power of the mode with lower (higher) optical frequency. (From [42])

effective anisotropies is an examination of optical spectra. The frequencies and the widths of the peaks that correspond to the lasing and the non-lasing mode are related to the effective birefringence and dichroism, respectively, as follows: The difference in frequency corresponds to the effective birefringence. The difference in linewidth (HWHM) of the lasing and the non-lasing mode corresponds to the effective dichroism [14].

A second method is the analysis of polarization fluctuations in RF-spectra by a homodyning method. After a suitable mixing of the polarization components on a fast detector, the central frequency of the beating peak in the RF-spectrum corresponds to the effective birefringence and the HWHM of the peak corresponds to the effective dichroism [14, 39]. Details can be found in [14, 39]. This method is more precise than the method based on optical spectra since there is no limitation set by the finite finesse of a FPI.

# 3   EXPERIMENTAL RESULTS

## 3.1   Polarization switching from the high-frequency to the low-frequency mode

### 3.1.1   General scenario

First, we are going to consider PS from the HF to the LF-mode. Fig. 2 depicts the stability regions of the two polarizations modes in the form of polarization resolved light-current (LI) characteristics plotted for different substrate temperature for one of the devices under study.

At about room temperature, the lasing emission at threshold is only in the polarization direction corresponding to the HF-mode, i.e., the lasing emission is purely linearly polarized. At increasing current, a PS to the LF-mode is observed, as it has been often reported in literature. If the substrate temperature of the device is increased, the current value of the PS moves closer to threshold. With increasing substrate temperature this development continues

7

until finally the point of excitation of the LF-mode coincides with the lasing threshold (at about 60°C). This leads to emission of both polarizations at threshold. We will refer to this as *two-frequency emission* (TFE) for reasons which will become clear in Sect 3.1.3. At increasing current, the mode with higher optical frequency is depleted until only the LF-mode is lasing. If the substrate temperature is increased even further, the emission at threshold is dominated by the LF-mode.

This trend closely follows the temperature dependence of the dichroism at threshold. In the regime of excitation of both polarizations at threshold, the absolute value of the dichroism is less than 0.05 GHz, at 10°C it is about 0.3 GHz. Thus, the observation can be interpreted in the following way. For low temperatures, the linear dichroism favors the HF-mode, for high temperatures the LF-mode. In between there is a change of sign of dichroism. In the vicinity of the zero, both polarization modes are on (nearly) equal footing. Hence, both can be excited on time average. As stated above, in general it is difficult to extract the origin of the linear dichroism directly from the measurements. However here, the fact that the change between the dominance of the HF and the LF-mode occurs in or in the close vicinity of the threshold minimum hints to the *gain dispersion mechanism* proposed by Choquette et al. [11, 16] as the dominant effect. The basic idea behind this is quite simple: Since the two polarization modes are typically split in frequency (here the birefringence is 6 GHz) they will experience a slightly different gain. If the gain maximum has a higher frequency than the (average) longitudinal cavity resonance, the HF-mode will be favored, otherwise the LF-mode. If the device temperature is changed, the detuning condition changes since the wavelength of the gain maximum and the cavity resonance shift with quite different rates with temperature (about 0.3 nm/K for the gain [16, 43], 0.08 nm/K for the cavity resonance). In a first approximation (i.e., neglecting the decrease in gain and the increase in relaxational processes with increasing temperature), the position of minimal threshold for the fundamental mode will be the temperature were gain maximum and cavity resonance are aligned. Hence different polarization modes can be expected to be dominant on the different sides of the threshold minimum as seen in Fig. 2 (see also [11, 16]).

In the following, we will discuss details of the polarization switching at low temperature (Sect. 3.1.2) and of the TFE-regime at high temperature (Sect. 3.1.3).

### 3.1.2   Polarization switching

Figure 3a displays the polarization resolved LI-curve under cw-operation for a device temperature of 10°C. At threshold the light is emitted in the HF-mode. A PS to the LF-mode is observed at 11% above the threshold current. At the PS a small decrease of the output power of approximately 3% is observed, i.e., the LF-mode has a lower emission power than the orthogonally polarized mode at the point of the PS. A linear interpolation of the power of the LF-mode intersects the current axis at a current value that is higher than the lasing threshold, which is the threshold of the HF-mode. This indicates that the LF- mode has a higher threshold. This observation is remarkable, since lasers normally tend to choose the state with the highest output power, if mode selection is only due to the balance of linear (unsaturated) gain/loss anisotropies. Hence, this is an indication that a treatment based solely on linear anisotropies is not sufficient.
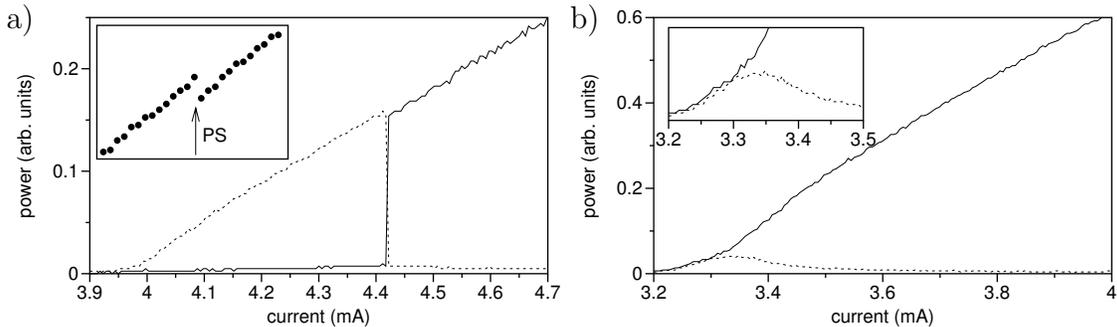
Figure 3: Polarization resolved output power in dependence of the injection current. a) PS at a substrate temperature of 10°C. The inset displays a magnification of the total output power (dotted line) in the vicinity of the PS, measured without polarization sensitive optics. b) TFE at a substrate temperature of 61°C. The inset shows a magnification of the current interval around threshold. (From [42, 44])

In order to ensure that the observed decrease of power is not due to a residual anisotropy of the analyzing polarization optics, we have placed a low bandwidth detector directly after the collimation lens. The total output power obtained from this measurement exhibits a abrupt decrease at the PS in accordance with the polarization resolved experiments (see inset in Fig. 3a). This is confirmed further by a measurement of the relaxation oscillation (RO) frequencies, which shows a stepwise decrease at the PS point indicating a decrease in intra-cavity power.

The scenario described up to now is observed for substrate temperatures of the VCSEL ranging from 6°C to 55°C, i.e. the temperature value up to which a clear, discontinuous PS can be observed (further details can be found in [44]). Thus, the PS is a robust phenomenon observed in a temperature range of almost 50°C. However, the increase of the active zone temperature with current is only 3°C to 4°C per mA and the observed PS occurs at current values less than 1 mA above the lasing threshold, i.e. the temperature increase before the PS should be less than 5°C. This is an indication that the PS observed in this VCSEL is not due to the mechanism proposed in [11, 16], i.e. not due to the fact the temperature of the active zone crosses the temperature for optimal alignment of gain and cavity resonance due to Ohmic heating. This is confirmed by the fact that a PS is also observed, if the VCSEL is biased below threshold and driven in addition by current pulses with a width of 10-50 ns – shorter than the relaxation time of the lattice temperature [17, 18] – and a low duty cycle of 1 kHz [37, 45]. Here the increase of lattice temperature due to the pulses is negligible. However, effects due to the change in plasma temperature [30] cannot be excluded. Polarization switching from the HF to the LF-mode at constant lattice temperature of the active zone were reported before [17, 29], but in these papers no drop of output power at the PS is mentioned. The existence of drop in output power after a PS was, however, recently reported also for optically pumped long-wavelength VCSELs [46].
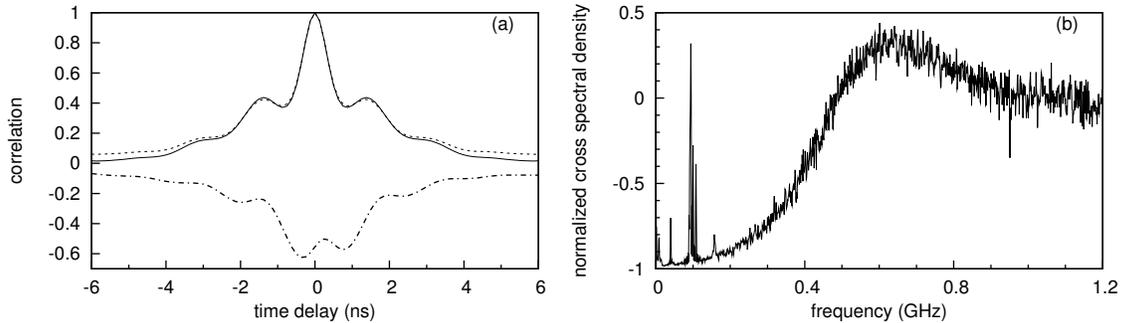
Figure 4: Correlation properties of the dynamics 4% above threshold in the TFE-regime. a) The solid (dashed) line displays the auto correlation function of the mode with lower (higher) optical frequency, the dash-dotted line represents the cross correlation function of the two modes. b) Normalized cross spectral density. The fluctuations visible for frequencies less than 150 MHz are induced by perturbations due to broadcast radio signals. They have been checked to enter into the APDs and to appear also if the output of the VCSEL is blocked. (Adapted from [42])

### 3.1.3 Two-frequency emission

Figure 3b shows the polarization resolved LI-curve with the substrate temperature set to 61°C in greater detail. At threshold, both of the orthogonal polarization modes start to lase with equal time averaged power. Up to approximately 4% above threshold the power increases equally for both modes. Then a preference for the LF-mode is observed, though the power in the HF-mode still increases up to nearly 6% above threshold. For further increasing current the power in this mode continuously decreases until it reaches the spontaneous emission level. The time-averaged optical spectrum at threshold shows two peaks of equal magnitude with orthogonal linear polarizations corresponding to the two modes, i.e., the presence of power in both polarization directions can not be attributed to a single elliptically polarized lasing mode. Hence, we will call the current interval in which both modes are lasing *two-frequency emission* (TFE) regime. Dynamics, correlation properties and spectra of the two modes in the TFE-regime were investigated in detail in [42]. Here we review only the main findings.

At threshold, in both polarization directions bursts starting from the spontaneous emission level are observed. The amplitude of the fluctuations is of the same order of magnitude as the average power. The bursts have amplitudes of an equal order of magnitude for both polarization components and appear with the same probability in a fixed time interval. This corresponds to the fact that the time averaged power was observed to be equal for both polarization modes. In the RF-spectra, relaxation oscillation (RO) peaks are observed for both modes. This is a confirmation that both modes are lasing. If the current is increased beyond 4% above the threshold value, the bursts in the HF-mode appear less frequently than the ones in the other mode and their amplitude decreases, until – at high currents – the lasing LF-mode is fluctuating around a DC-level and the non-lasing HF-mode shows only small-amplitude fluctuations on the spontaneous emission level.

10

In Fig. 4a, the correlation properties of the time series at 4% above threshold in the TFE-regime are shown. The auto correlation functions of both modes exhibit a distinct modulation with the frequency of the RO. This modulation is also present in the cross correlation function of the dynamics. The cross correlation function reveals a clear anti-correlation of the dynamics in the two polarization directions and is slightly asymmetric with respect to zero time lag. The (anti)correlation decays to zero within a few nanoseconds. The absolute value anti-correlation increases with current and reaches a value of -0.72 at $I = 3.36$ mA. Afterwards, i.e. if the depletion of the HF-mode sets in, it decreases again.

To clarify the influence of the different frequency components on the dynamics, we have computed the normalized cross spectral density (NCSD) of the two time traces $I_{x,y}(t)$ of the polarization components by Fourier transformation (denoted in the formula below by a tilde) and use of the relationship

$$C(f) = \text{Re}\left[\frac{\tilde{I}_x(f) \cdot \tilde{I}_y^{\star}(f)}{\sqrt{|\tilde{I}_x(f)|^2|\tilde{I}_y(f)|^2}}\right] . \tag{1}$$

The NCSD contains information about the amount of (anti)correlation at a certain frequency. The results are given in Fig. 4b. At low frequencies, the dynamics are almost perfectly anticorrelated except for technical noise. This corresponds to the overall anticorrelation at zero time lag in the cross correlation function in the time domain (see Fig. 4a) and the rather slow decay of the anticorrelation for larger time lags. Anticorrelation at low frequencies has been shown to be a robust feature of the polarization dynamics of VCSELs in past investigations [47, 48]. For increasing frequencies, the correlation increases (i.e., the modulus of the anticorrelation decreases) until the NCSD reaches a maximum at 0.6 GHz with a normalized correlation value of about 0.3. At further increasing frequency, the NCSD decays towards zero. The frequency of the maximum corresponds to the RO frequency of the total power. Since the RO are a process that acts on the total inversion and both polarization modes are lasing in the regime under study, they have to be influenced simultaneously.

This observation explains why the anticorrelation at zero time lag shown in Fig. 4a is not complete (i.e., -1) although the NCSD at low frequencies is perfect: at zero time lag we have a contribution from all the frequency components of the NCSD, the high-frequency components reducing the anticorrelation due to the low-frequency ones.

We will argue later that the TFE is the manifestation of bistability between the two polarization state in a situation very close to threshold where noise plays a particularly strong role due to the weak damping of the relaxation oscillations and the strong influence of the spontaneous emission.

### 3.1.4   Some aspects of the dynamics of polarization switching

In this section, we are going to give some additional information on the dynamical aspect of polarization switching.

First, Fig. 5a shows that there is hysteresis around the PS point, i.e., the switching points differ, if the current is increased or decreased. This indicates that there is bistability between

the two polarization modes within the hysteresis loop. This might open the possibility of using polarization to encode or process information and use VCSELs for an all-optical processing of these data (e.g. [49, 50]). However, the width of this hysteresis loop is usually quite small, only about 20 $\mu$A in this example which can be regarded as typical. We mention that this changes drastically, if high order transverse modes are present in the switching process. In that case hysteresis loops can reach several mA [51].
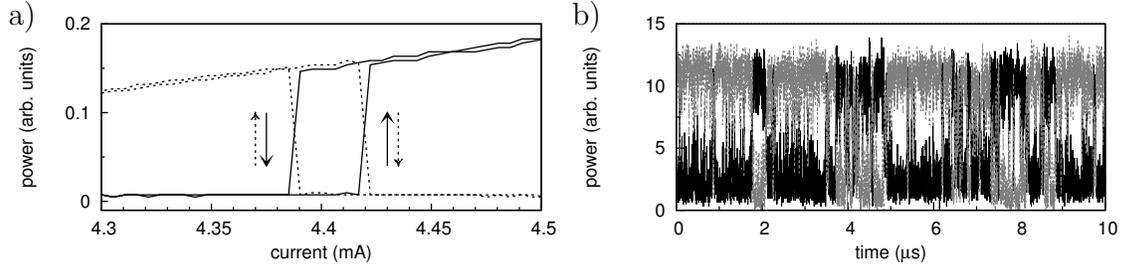


Figure 5: a) Polarization resolved LI-curve including the measurement for increasing and decreasing current (substrate temperature 10°C). The arrows indicate the direction of the polarization switching. The scanning time for the complete measurement is 160 seconds. b) Time series with a cw bias within the bistable range (substrate temperature 40°C, grey line LF-mode, black line HF-mode).

Since it is known that the width (or even the apparent existence) of a hysteresis loop might depend on the ramping speed of the stress parameter due to phenomena like critical slowing-down (e.g. [52, 53]), the existence of bistability was confirmed by biasing the laser at a working point within the hysteresis loop and looking for noise-induced transitions between the two states. Fig. 5b shows a time series displaying a square-wave like hopping between the two linear polarization states. Plotting histograms of the amplitude distribution of each of the two polarization components yields double-peaked (so-called 'bimodal') distributions [54] which are a proof of bistability (e.g. [55] and Refs. therein). Since the properties of the stochastic hopping dynamics within the bistable range are treated intensively in the literature (e.g. [26, 56, 57]), we do not go into details here. We mention that the cross correlation function reaches -1 at a time lag of zero and decays then slowly within a few hundred ns towards zero. This reflects the fact that the time scale of the competition dynamics is 100 ns to microseconds. This longer time scale and the square-wave shape of the envelope is the distinct difference to the dynamics in the TFE-regime. The additional difference is that the modulations due to the ROs are no longer pronounced since the damping of the ROs increases with increasing distance to threshold.

Looking at a single switching event, it turns out that the 'switching time', i.e., the transition time to the new polarization state defined by a 10%-90%-criterion, lies in the range between one nanosecond and some nanoseconds depending on parameters [54]. This is in accordance with results from other groups [58, 59]. The same time scale applies for a PS induced by sweeping the current sufficiently far beyond the limit point of the bistable region. It should be noted, however, that the observation of this short time scale does not allow any claim on a non-thermal origin of the switching, because the thermal contribution might be hidden in a long lethargic stage in which the system is very close to the original state. This initial

12

stage is not captured by a 10%-90%-criterion. Only modulations experiments [29] or pulsed excitation (see above) can help to distinguish between thermal and non-thermal origins of the PS.

## 3.2 Polarization switching from the low-frequency to the high-frequency mode

Apart from the PS type 1 discussed in last section, switching from the LF to the HF-mode (so-called 'PS of type 2') is described also in the literature [14, 20, 58, 60, 61]. It is instructive to compare the properties of type 1 and type 2 switching since the SFM allows for both, but gives definite different predictions for the two cases [23].

Fig. 6a shows a LI-characteristic with a PS of type 2 for one of our devices. Interestingly, for projection onto orthogonal linear polarization components there is always also significant excitation of the weaker polarization. This is due to the fact that the lasing mode is in fact elliptically polarized, as it can be shown by a measurement of the Stokes parameter, (ellipticity angle at threshold 10.5°, see Fig. 7a of [51]). Far enough away from the PS, the *fractional polarization*, i.e. the sum of the squares of the normalized Stokes parameters, is nearly one (Fig. 6b), i.e. there is a still a pure – though elliptical – SOP. Another difference to the scenario discussed in the preceding section is that the fractional polarization drops to rather low values in a rather broad interval around the PS point. This indicates that there is no pure polarization state in this regime. Indeed, in the optical spectrum there are multiple lasing lines with elliptical polarization but different principal axes (see Fig. 2 of [60]). This indicates that the emission of the laser is not constant but that there is a *dynamical, self-pulsing state*. We will discuss details below. We never observed such a behavior for a PS of type 1.
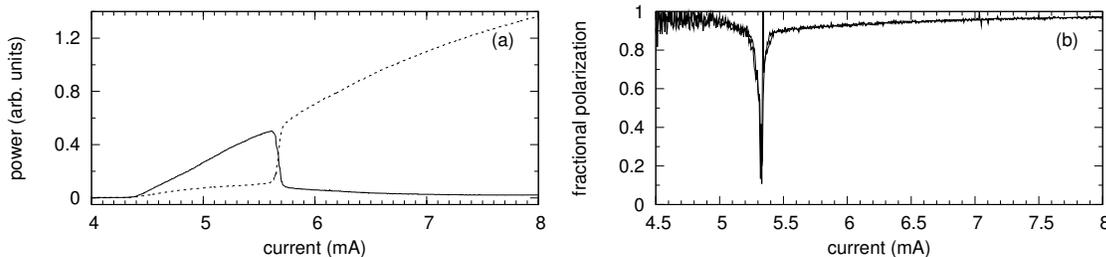


Figure 6: a) LI-curve after projection on linear polarization states with the axes parallel to the principal polarization axes at the PS. Substrate-temperature 15.9°C. b) Fractional polarization. The vertical line denotes the PS point. The strong noise for low current is due to the fact that the signal level is small. Substrate temperature: 22.6°C. (Adapted from [51, 60])

This behavior is rather robust. The LF-mode is the mode selected at threshold for the whole temperature range investigated (10° − 65°C, see Fig. 5 of [61]). At high currents, the HF-mode is active. In between, there is the PS with the transition region with dynamical states.

The region with dynamical states is sickle-shaped and closes, in tendency, for increasing temperature.

In the laser, in which the SOP is elliptically at threshold, the principal axes of the SOP are not aligned to the wafer axes and rotate continuously with current by a rather large amount, about 15° (see Fig. 7a of [51]; the principal axis of a 'linear' (see Sect. 2) SOP are fixed within 1° or less). This hints to the fact that the principal axis of birefringence and dichroism are not aligned in these devices as discussed in Sect. 2. For a comparison between theory and experiment as well as between PS of type 1 and PS of type 2, it is an important question, whether the dynamical states can also be observed experimentally for other parameter values, i.e., for other values of linear dichroism and birefringence and especially for lower values of the ellipticity angle of the steady state at threshold. To induce the parameter changes, stress was applied to different devices with the method explained in Sect. 2. With this method the linear anisotropies were changed until a PS from the LF-mode to the HF-mode occurred. The results are summarized in [61].
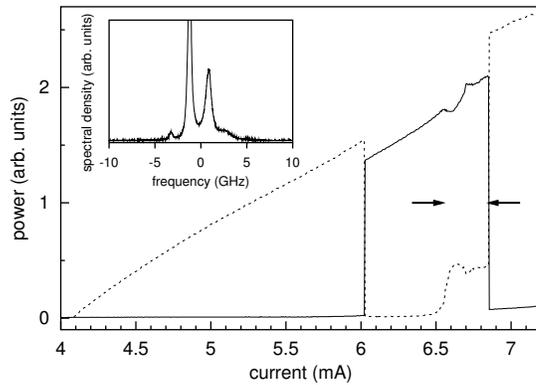


Figure 7: Polarization resolved output power against current for projection onto the main axes of the state of polarization at threshold for a device with an ellipticity angle ≤1° at threshold. The inset shows the optical spectrum for a current of 6.66 mA after projection onto linear polarization. The largest peak is cut off for a better visualization of the smaller peaks. The arrows denote the current region in which sidebands are observed in the optical spectrum. (From [61])

Here, we will discuss in detail a particularly interesting scenario which is depicted in Fig. 7. At threshold, the lasing mode is the HF-mode. The SOP can be regarded as linearly polarized, the ellipticity angle is smaller than 1° (see the discussion at the end of Sect. 2). At increasing current, at first a PS to the LF-mode occurs (note the drop in power). Up to a current of 6.5 mA – i.e., in a current range extending beyond the first PS – the ellipticity stays below 4°. Also dynamical states do not appear at the first PS. If the current is increased further (beyond 6.5 mA), the ellipticity angle strongly increases (see also the increase of power in the weak linear polarization component about 6.4 mA) and reaches about 22° before the second PS. At a current value of 6.55 mA sidebands appear in the optical spectrum and the fractional polarization decreases strongly (the minimum value is about 0.6). The sidebands disappear at the second PS, which is a switching back to the HF-mode. The

14
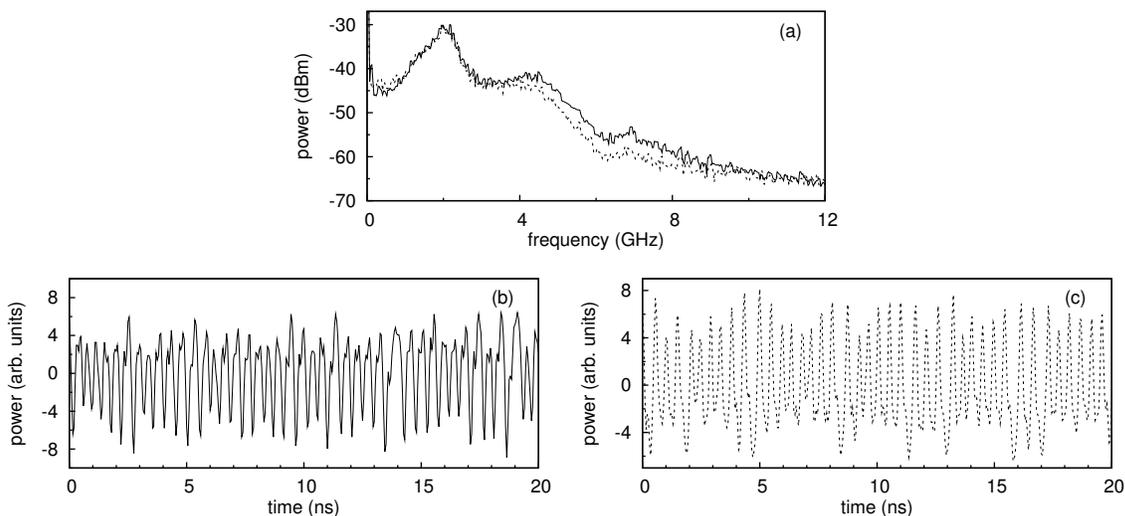
Figure 8: Power spectra (a) and time series (b,c) of the dynamics in the regime of the emission of dynamical states. The solid (dashed) line in (a) represents the power spectrum after projection onto the linearly polarized state with maximum (minimum) dc-output. The corresponding time trace is given in (b) and (c), respectively. All data were measured after 40 dB amplification. Note that the two time traces have not been obtained simultaneously and that the DC-information is lost due to the amplification. (Adapted from [61])

fractional polarization increases again after the PS and the ellipticity drastically decreases. This scenario reported here is qualitatively similar to the one observed for a single PS from the LF- to the HF-mode [61].

The results obtained so far indicate that the existence of elliptically polarized dynamical states before a PS of type 2 does not depend qualitatively on the initial ellipticity of the SOP at threshold, i.e., the scenario for the destabilization of the LF-mode is: LF-mode lasing (nearly linearly polarized) → increase of ellipticity → appearance of multiple peaks in the optical spectrum and drop of fractional polarization → PS to HF-mode. As we will see later, these observations confirm the core of the predictions of [23] for the transition scenario.

In some of the experiments a fast digital oscilloscope was available, allowing for an investigation of the temporal dynamics during the emission of the dynamical states. In Fig. 8 the dynamics is illustrated for the same device that is presented in Fig. 6 but for a different run of the experiment. As depicted in Fig. 8(a), a strong peak at a frequency of about 2.1 GHz is observed in the power spectrum for projection onto the linear polarization directions corresponding to maximum and minimum time averaged power, i.e., onto the main axes of the polarization ellipse of the time averaged SOP. This frequency corresponds to the distance of the sidebands in the optical spectrum (in optical frequencies) and can therefore be interpreted as the beating frequency between the different 'modes' which are oscillating at adjacent frequencies. We interpret this frequency difference as the 'effective birefringence', i.e., the sum of the linear birefringence observed at threshold and the non-linear contributions due to saturable dispersion and spin dynamics [14,38,39,60,62]. Since several sidebands are excited in the optical spectrum (see also inset of Fig. 6), also higher harmonics of the beating frequency are observed in the power spectrum.

15

Corresponding to these frequencies, pronounced oscillations are observed in the time domain (see Fig. 8(b) and (c)). The time traces have not been obtained in a simultaneous measurement. Hence they contain no information about the correlation properties of the dynamics. The oscillation at 2.1 GHz is observed for projection onto both of the polarization main axes.

From these observations the following conclusions can be drawn: First, due to the rather regular temporal oscillation at the frequency splitting of the sidebands in the optical spectrum, the sidebands can be considered as a (nearly) locked state and not as independent modes. Second, the presence of these oscillations in both linear polarization components hints to an oscillation of the characteristic polarization angles, i.e., ellipticity and orientation of the SOP. This issue is discussed further in the theoretical section.

# 4   THEORETICAL INVESTIGATIONS AND DISCUSSION

## 4.1   Model equations

The experimental observation clearly indicate two important features any model should be able to explain (apart, of course, from the obvious fact that there is polarization switching):

- The ellipticity of the optical field was observed to vary. Hence, one has to take into account the *relative phase* between the two polarization components and thus needs to treat equations for the complex optical fields, not only the intensities as often done in the literature.

- The model should include the possibility that switching occurs to the mode with the lower unsaturated gain, it should not concentrate on a change of the linear gain-loss balance as the basic mechanism behind polarization switching.

To our knowledge, the spin-flip model [22, 23] is the only model worked out in the literature which is capable of fulfilling these requirements. Especially, dynamical states have not been reported in the framework of other models until now. In particular, we will use an extended version of the spin-flip model that includes a realistic semiconductor susceptibility [63, 64]. Thanks to the frequency dependence of the susceptibility one is capable to correctly describe changes in the relative position between the cavity resonance and the gain curve. Hence, the thermal shift of resonances due to temperature changes, which is important, e.g. for an explanation of the observations depicted in Fig. 2, can be easily taken into account. It will turn out that it is possible to explain all the observations presented before in a single model using essentially the same parameters except for the linear anisotropies, which obviously have to be adjusted to any new situation [42, 44, 61]. This does not exclude that it is possible – and interesting – to describe important aspects of a particular phenomenon by a reduced set of equations derived from the SFM (e.g. [65] for PS of type 1 and [66] for PS of type 2).

Under fundamental transverse mode operation, the evolution of the circularly polarized components of the electric field $E_\pm$ (slowly-varying envelopes) and the electronic densities

16

$D_\pm$ with opposite spin (normalized to the transparency density $N_t$) are governed by [63,64]:

$$\dot{E}_\pm(t) = -\kappa E_\pm + i\frac{a\Gamma}{2}\,\chi_\pm\left(\Omega + i\frac{\dot{E}_\pm}{E_\pm}, D_+, D_-\right)E_\pm - (\gamma_a + i\gamma_p)E_\mp + \sqrt{\beta_{sp}D_\pm}\xi_\pm(t), (2)$$

$$\dot{D}_\pm(t) = \frac{1}{2}\mu\frac{I_t}{eN_t} - AD_\pm - BD_\pm^2 \mp \gamma_j(D_+ - D_-) + a\cdot Im\chi_\pm\left(\Omega + i\frac{\dot{E}_\pm}{E_\pm}, D_\pm\right)|E_\pm|^2. (3)$$

The electronic densities with opposite spin interact with circularly polarized light with different helicity through the frequency dependent susceptibility $\chi_\pm$ [63,67]. We use analytical expressions for $\chi_\pm$ obtained in [67] that describe the gain and refractive index spectra as

$$\chi_\pm(\omega_\pm + \Omega, D_\pm) - \chi_0 \left[\ln\left(1 - \frac{2D_\pm}{u_\pm + i}\right) + \ln\left(1 - \frac{D_+ + D_-}{u_\pm + i}\right) - \ln\left(1 - \frac{b}{u_\pm + i}\right)\right] \quad (4)$$

where

$$u_\pm = \frac{\omega_\pm}{\gamma_\perp} + \Delta + \sigma(D_+ + D_-)^{1/3} \quad , \quad \Delta = \frac{\Omega - \omega_t}{\gamma_\perp} \quad . \quad (5)$$

$\Delta$ is the detuning between the cavity resonance $\Omega$ and the nominal transition frequency $\omega_t$ of the band gap, normalized to the material polarization decay rate $\gamma_\perp$. Thus, the difference in thermal shift of the frequency of the gain maximum and of the cavity resonance can be modeled by a variation of $\Delta$. $\Delta$ increases with temperature since the redshift of the cavity resonance increases faster with temperature than the redshift of the band gap frequency [16]. $\sigma$ describes band-gap shrinkage and $b$ is a background contribution to $\chi$ without pumping. Spin-flip processes that reverse the electron spin directly couple the two carrier reservoirs. This effect is phenomenologically accounted for by means of the spin-flip rate $\gamma_j$. $\mu$ is the injection current normalized to the transparency current ($I_t$), $e$ is the electron charge. The linear contributions to the birefringence and dichroism are $\gamma_p$ and $\gamma_a$, respectively. In the framework of this model $\gamma_a$ is a pure loss anisotropy. The differences in material gain due to the frequency splitting between the modes are incorporated by the optical susceptibility $\chi_\pm$. The rest of parameters are the cavity losses $\kappa$, the effective gain constant $a$, the confinement factor $\Gamma$, the non-radiative and bimolecular recombination rates of the carriers $A$ and $B$ and the spontaneous emission rate $\beta_{sp}$. Finally, $\xi_\pm(t)$ are white Gaussian random numbers with zero mean and delta correlated in time that model spontaneous emission processes.

For convenience, the simulations have been performed in the circular polarized basis. To obtain expressions for the linearly polarized components one has to use the relations $E_{||} = (E_+ + E_-)/\sqrt{2}$, $E_\perp = (E_+ - E_-)/(i\sqrt{2})$, where steady state solutions of $E_\pm$ are of the form $E_\pm(t) = Q_\pm e^{-i(\omega_\pm t \pm \psi)}$ with $Q_\pm$ being the amplitude of the field and $\psi$ the phase with which the circularly polarized fields lock. If $\gamma_p > 0$, $E_\perp$ corresponds to the LF-mode and $E_{||}$ corresponds to the HF-mode. The parameters used for the simulations are given in the figure captions and can be considered to be typical VCSEL parameters. The spin flip rate $\gamma_j$ is taken as a fit parameter. It is found that the experimentally observed dynamics can be reproduced, if a rather low value of some tens of $10^9$ s$^{-1}$ is assumed. We will comment on this below.

a)



b)
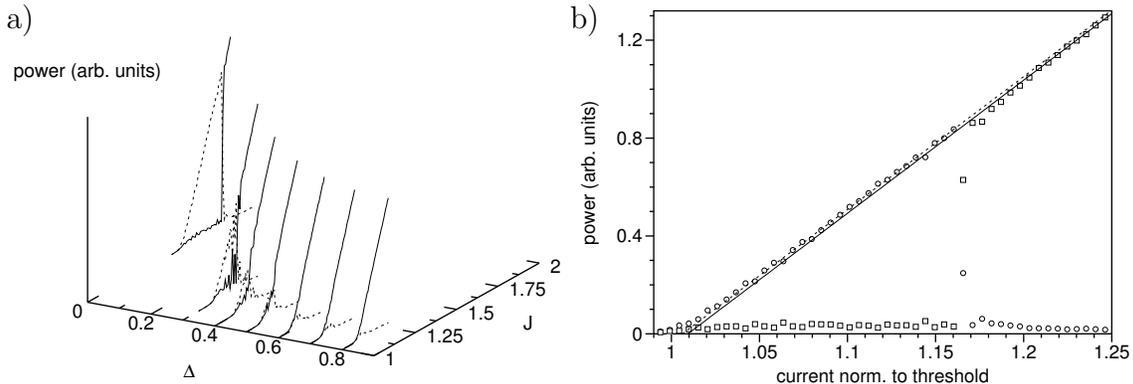


Figure 9: a) Polarization resolved output power in dependence of the detuning $\Delta$ and injection current $J$ normalized to its transparency value. The parameters defining the susceptibility function [67] are $b = 10^4$, $\gamma_\perp = 10^4$ ns$^{-1}$, and $\sigma = 0.2$, other parameters $\gamma_p = 18$ ns$^{-1}$, $\gamma_a = 0$, $\kappa = 300$ ns$^{-1}$, $a = 2.3 \cdot 10^4$ ns$^{-1}$, $\Gamma = 0.045$, $A = 0.5$ ns$^{-1}$, $B = 1.0$ ns$^{-1}$, $\beta_{sp} = 10^{-6}$ ns$^{-1}$, $\gamma_j = 20$ ns$^{-1}$. b) Polarization resolved LI-curve obtained from simulations for $\Delta = 0$. Circles (squares) denote the power in the mode with higher (lower) optical frequency. The dashed (solid) lines are linear fits applied to the data before (after) the PS. The integration time per point is 100 ns. (From [42,44])

## 4.2   Theoretical investigations on PS of type 1

First, we are going to consider the case of the destabilization of the HF-mode. As a first step, LI-curves for various detunings have been simulated (see Fig. 9a) assuming that there is no loss or strain induced dichroism, $\gamma_a = 0$. By a change of the detuning a variation of substrate temperature as performed in the experiments can be simulated. As it is obvious from Figs. 2 and 9a, the simulations reproduce the experimentally measured polarization properties qualitatively for variation of both the detuning *and* the current. The selection of the lasing mode at threshold is, of course, the result of the gain dispersion mechanism proposed by Choquette et al. [11, 16] and discussed in the experimental section.

In the discussion, we concentrate first on the situation for small detuning (corresponding to low temperature in the experiment). In Fig. 9b the simulated LI-curve for a detuning value of $\Delta = 0$ is displayed. At threshold the laser oscillates in the HF-mode, which is the one closer to the gain peak. If the current is increased beyond a value of 16% above the lasing threshold, a PS to the LF-mode is observed. Linear fits have been applied to the data before and after the PS (see lines in Fig. 9b). The fitting results reveal a drop of the output power at the PS and a higher threshold for the LF-mode, i.e. the PS is to the mode with lower gain. The decrease of power at the PS is of the order of 2%. In the simulations, the linear anisotropies were assumed to be unchanged during the current scan, but we can also include a current-dependent drift in $\Delta$ (and hence the gain anisotropy) in order to model the effects of Joule heating. As long as the increase of $\Delta$ with current is moderate the drop of the output power at the PS is still observed [44].

In the theory, we are in the favorable situation that there is no doubt on the interpretation of this power drop: The linearly polarized steady state solutions of the equations (2),(3) are functions of $\gamma_a$ and the imaginary part of the susceptibility. This results in general

18

in different thresholds for the two polarization modes and in different amplitudes of the linearly polarized fields at constant current [64]. Hence, the drop is a direct consequence of the fact that the mode with the higher unsaturated net gain becomes unstable in favor of the mode with the lower unsaturated net gain. Though this might sound counter-intuitive on the first sight, it is necessary to recall that the unsaturated net gain governs only the competition for growth from the non-lasing, zero solution, but not – at least not necessarily – from a lasing solution (see also [32]). The destabilization of the higher gain mode is due to a complex interplay of birefringence, phase-amplitude coupling and spin-flips [24]. This is, e.g., apparent from the contributions entering the cross-coupling coefficients between polarization modes coefficient in perturbative treatments [38, 62, 65]. However, no simple explanation seems to be available in the literature, though some insight can be gained by considering the trajectories of perturbations on the Poincare sphere [62]. We mention that similar effects are at work in *detuned gas lasers* (e.g. [68, 69]), the detuning being responsible for phase-amplitude coupling. Since in semiconductor lasers phase-amplitude coupling is particularly strong and, in addition, exists even for operation at the gain peak [25], the existence of these effects in VCSELs is not totally surprising.

A detailed comparison of the hysteresis properties and the development of the effective dichroism in experiment and theory is contained in [44]. Also there, the experimental results are in good qualitative agreement with the predictions of the SFM. The power drop at the PS is also contained in versions of the SFM which contain gain saturation ( [70], often called also 'gain compression'), or reduced versions of the SFM in which the processes of spin-flips and phase-amplitude coupling are 'condensed' in a cross-saturation coefficient [65]. It is also discussed in [44] that gain saturation alone [71, 72]– i.e. for zero linear dichroism – might explain bistability, but not the power drop. We also stress that the observation of a minimum of dichroism or mode suppression ratio [14, 29] is – taken alone – not sufficient to draw conclusions on the origin of the PS, i.e. whether it is solely induced by a change in linear dichroism or not [44].

In the TFE-regime, the important features of the dynamics, i.e., the overall shape of the time series, spectral and correlation properties, can be also reproduced nicely by the SFM [42]. The analysis shows – as expected intuitively – that the PS point moves to lower current values with increasing detuning (cf. Fig. 9a)) due to the reduction of the linear dichroism. In the threshold minimum, the two linear polarization modes are bistable already at threshold. In that situation, the apparent competition dynamics is particularly strong and takes place on short time scales, since close to threshold the influence of spontaneous emission noise is particularly strong and the relaxation oscillations are only weakly damped. Hence, TFE can be regarded as the manifestation of bistability close to threshold. Although the TFE-regime cannot provide a clear-cut distinction between the SFM and other models, since the correlation properties between polarization modes should resemble qualitatively the ones depicted in Fig. 4 in any model allowing for polarizing competition, the comparison between SFM and experiment is favorable even in a semi-quantitative way [42]. This is the more remarkable since a single set of parameters was used to describe the PS and the TFE dynamics. Finally, we mention that the depletion of the HF-mode further above threshold is due to nonlinear contributions to the dichroism [42].
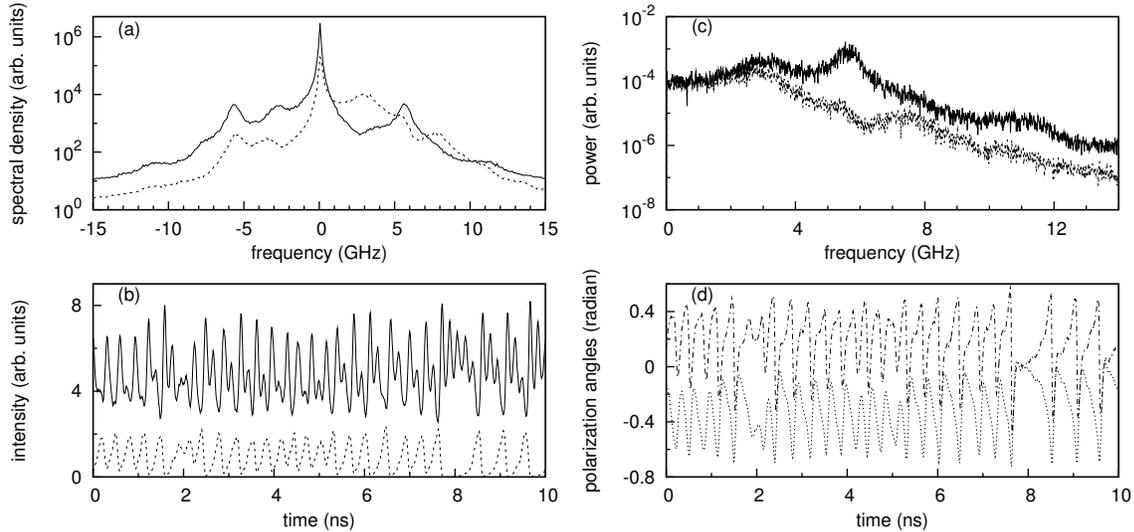
Figure 10: Spectra and temporal evolution for projection onto linearly polarized states during the emission of the dynamical states. The optical spectra are shown in (a). The temporal evolution of the corresponding field intensities is displayed in (b), whereas in panel (c) the power spectrum calculated from the time traces (total integration time 2 $\mu$s) is shown. The temporal evolution of the polarization angles is given in (d), where a dotted (dash-dotted) line represents the ellipticity (orientation) angle of the state of polarization. The parameters are $\gamma_a$=1 ns$^{-1}$, $\gamma_p$=9 ns$^{-1}$, $\gamma_j$=20 ns$^{-1}$, $\Delta$=0, $A$=0.5 ns$^{-1}$, $B$=1 ns$^{-1}$, $\kappa$=300 ns$^{-1}$, $a = 2.5 \times 10^4$ ns$^{-1}$, $\gamma_\perp = 10^4$ ns$^{-1}$, $\beta_{sp}$=10$^{-6}$ ns$^{-1}$. The current is 1.9 times the threshold value. (Adapted from [61])

## 4.3  Theoretical investigations on PS of type 2

As mentioned above, the SFM makes a definite prediction for the destabilization of the LF-mode in a broad parameter regime [23]: The linearly polarized LF-mode becomes unstable in favor of an elliptically polarized modes at some point, if the current is increased above threshold. At a somewhat larger current, the elliptically polarized modes becomes unstable, too, and regular oscillations develop. If the current is increased further, these oscillations become irregular, possibly chaotic, until finally the system switches to the linearly polarized HF-mode. Details of this scenario are investigated semi-analytically in [73, 74]. Due to the complexity of the extended SFM used here, it is more difficult to determine the elliptically polarized solutions and their stability. Hence we performed only numerical simulations.

Details can be found in [61]. LI-curves and the existence regions of dynamical states are found to be in qualitative agreement with experimental observation. Here, we will discuss only the time series in the presence of dynamical states. Typical results are depicted in Fig. 10.

Panel (a) displays the optical spectra after projection onto linearly polarized states, which exhibits several sidemodes that are typical for this dynamical regime. This matches the experimental observation (see Fig. 8) except for the amplitudes of the sidebands, which are considerably more excited in the experiment. The time traces of the corresponding intensities are given in panel (b) and the power spectra in panel (c) of Fig. 10, respectively. As in the

20

experiments, the power spectra exhibit pronounced components at the beating frequency of adjacent side modes and its multiples. The corresponding oscillations are observed in the time traces. The computation of a cross correlation function reveals that the intensities in the orthogonal linear polarization directions have a correlation of -0.76 at zero time delay, i.e., they are strongly anticorrelated. As in the experiment, the oscillations are rather – but not totally – regular.

Unlike in the experiment, in the simulations the time resolved ellipticity and orientation angle can be easily computed from the time series of the complex optical field components. The result of this procedure is displayed in Fig. 10d. Both polarization angles are strongly oscillating. Their oscillation is also strongly anticorrelated. The fractional polarization has a value of 0.45. Thus these oscillations can be interpreted as an oscillation on the Poincare sphere (see also [23, 62]).

Obviously, the destabilization scenarios are strikingly different for the HF-mode and the LF-mode. In our opinion, the asymmetry is due to the different mechanism of destabilization of the lasing mode. The linearly polarized steady state is characterized by equality of $D_+$ and $D_-$ [23, 64], which is valid for both the LF- and the HF-mode. For linearly polarized states, the stability of the total intensity decouples from the stability of the polarization subset. The stability of the linearly polarized modes against perturbations with orthogonal polarization and/or a deviation from $D_+ = D_-$ is expressed by the three remaining eigenvalues. Two of these are complex conjugate, the third eigenvalue is real. The real eigenvalue is (at least in the case of relatively large spin relaxation rates) mainly associated with perturbations of the equality of $D_+$ and $D_-$ [38, 62]. In the case of switching from the HF- to the LF-mode and for the parameter combinations we have studied, it is always the complex conjugate eigenvalue that acquires a positive real part and hence leads to destabilization of the HF-mode (see also [23]). The real eigenvalue is always negative, what implies stability of the condition $D_+ = D_-$. Elliptically polarized steady states are characterized by $D_+ \neq D_-$ [23]. Hence, elliptically polarized states cannot be expected.

For the PS from the LF- to the HF-mode, the behavior of the eigenvalues is different. Here it is the real eigenvalue which becomes unstable, possibly after the imaginary part of the complex conjugate eigenvalues became before zero at increasing current. This explains somehow the tendency to form an elliptically polarized state with $D_+ \neq D_-$.

Looking more on physical mechanisms (than eigenvalue analysis), an asymmetry between the LF- and HF-mode exists in the framework of the SFM, since the nonlasing mode experience a redshift above threshold related to phase-amplitude coupling [14, 38]. Hence, the effective birefringence increases, if the HF-mode is lasing, as observed experimentally in [14]. On the contrary, if the LF-mode is lasing, the splitting decreases (in tendency; the scenarios can be very involved depending on parameters, especially the spin-flip rate), which was indeed observed experimentally in our group [60]. It appears to be somehow intuitive that a decrease of the birefringent splitting favors the stable 'locking' to an elliptically polarized mode.

## 4.4   Influence of the spin-flip rate

The experiments and the simulations show good agreement for type 1 as well as type 2 switching, if the spin flip rate is assumed to be of the order of some tens of $10^9$ s$^{-1}$. Pre-

vious estimations of the spin flip rate under lasing conditions were inferred indirectly from experiments assuming the validity of the SFM and yielded $\gamma_j \approx 30 \ldots 75 \cdot 10^9$ s$^{-1}$ [75], $\gamma_j > 100 \cdot 10^9$ s$^{-1}$ [14], $\gamma_j \approx 10^{12}$ s$^{-1}$ [76] and 'infinity' [77], i.e., the values reported in the literature span over a rather wide range but are significantly higher, in tendency, than the values considered here. In that case, type I switching is indeed only possible, if a current dependence of the linear net gain is assumed. Also the current for PS of type 2 increases until it cannot be reached any more at a current value reasonable for real devices.

On the other hand, pump-probe experiments on passive quantum well structures yielded even lower values of $\gamma_j \approx 7 \ldots 9 \cdot 10^9$ s$^{-1}$, even at room temperature [78, 79]. However, it is often argued that it is doubtful whether these values provide a good estimation for the situation of a high carrier density typical for laser operating conditions. Nevertheless, at least one investigation demonstrates nearly circularly polarized lasing emission in a VCSEL after optical pumping with circularly polarized light [80]. Even though the data indeed demonstrate that the spin-flip rate increases with increasing carrier density, the lifetime of spin polarization at the laser threshold ($N_c \approx 3 - 4 \times 10^{18}$ cm$^3$) was found to be 40 ps, i.e., compatible with our assumptions. Hence we conclude that the assumptions made here on the spin-flip rate are well within the established limits.

The very different conclusions drawn in the literature on the relevance of spin-flip processes for polarization selection in VCSELs are probably related to the fact that the spin-flip rate depends on sample quality via the density of scattering centers [81]. Hence we regard our results as complementing – and not contradicting – the earlier investigations.

# 5   SUMMARY AND OUTLOOK

In this paper, we presented experimental results on polarization dynamics in VCSELs and their interpretation. The results, especially the observation of self-pulsing, elliptically polarized emission states and the switching to a gain disfavored mode, indicate clearly the need for taking into account phase degrees of freedom and nonlinear effects going beyond the normal 'winner take all' dynamics of the mode with the largest unsaturated, linear gain. Good agreement was found with the spin-flip model assuming a rather low spin-flip rate of some tens of $10^9$ s$^{-1}$. This is taken as a strong – though indirect – indication that spin dependent processes contribute to the polarization selection in the devices under study. Further insight is probably difficult to achieve with ready-made commercial devices but depends on the availability of wafer samples on which first-hand growth characterization, pump-probe characterization of the active zone in single pass, lasing properties with polarized optical pumping and lasing properties with electrical pumping are accessible at the same time. The results might be awarding in terms of *spintronics* and all-optical polarization based processing devices, even if for polarization control an enhancement of the linear dichroism might be the simplest option in the end.

Particularly interesting is also the interplay of polarization and transverse mode dynamics. VCSELs are also very vulnerable to the excitation of high-order modes, because typically the Fresnel number of the cavity is rather large. The appearance of high-order transverse modes is often accompanied by polarization effects (e.g. [9, 11, 15, 51, 82–84]). Some preliminary

results on the coupling of spatial and polarization degrees of freedom are found in [51]. Extensions of the SFM to a system of nonlinear partial differential equations for the study of transverse multi-mode dynamics are available [85, 86]. The polarization properties of spontaneously formed spatial patterns in broad-area VCSELs are also intriguing [87–90] and deserving further studies.

# ACKNOWLEDGEMENTS

# References

[1] J. J. Jewell, J. P. Harbison, A. Scherer, Y. H. Lee, and L. T. Florez. IEEE J. Quantum Electron. **27**, 1332–1346 (1991).

[2] K. J. Ebeling. *Analysis of vertical cavity surface emitting laser diodes (VCSELs)*. In A. Miller, M. Ebrahimzadeh, and D. M. Finlayson, editors, *Semiconductor quantum optoelectronics: From quantum physics to smart devices*, pages 295–338. SUSSP Publications and Institute of Physics Publishing, Bristol (1999).

[3] K. Iga. IEEE J. Selec. Top. Quantum Electron. **6**(6), 1201–1215 (2000).

[4] D. Wiedenmann, R. King, C. Jung, R. Jäger, R. Michalzik, P. Schnitzer, M. Kicherer, and K. J. Ebeling. IEEE J. Selec. Top. Quantum Electron. **5**(3), 503–511 (1999).

[5] C. Affolderbach, A. Nagel, S. Knappe, C. Jung, D. Wiedenmann, and R. Wynands. Appl. Phys. B **70**, 407–413 (1999).

[6] H. P. Zappe, F. Monti di Sopra, H.-P. Gauggel, K. H. Gulden, R. Hövel, and M. Moser. Proc. SPIE **3945**, 106–116 (2000).

[7] R. L. Thornton. Vertical-cavity lasers for high-density optical data storage. In *Photonics West (Vertical Cavity Surface-Emitting Lasers V)*, SPIE - The International Society for Optical Engineering, San Jose, CA, USA (2001). Paper 4287-27 (invited).

[8] M. Grabherr, M. Miller, R. Jäger, R. Michalzik, U. Martin, H. J. Unold, and K. J. Ebeling. IEEE J. Selected Topics Quantum Electron. **5**(3), 495–502 (1999).

[9] Hua Li, T. L. Lucas, J. G. McInerney, and R. A. Morgan. Chaos, Solitons & Fractals **4**, 1619–1636 (1994).

[10] Z. G. Pan, Shijun Jiang, M. Dagenais, R. A. Morgan, Keisuke Kojima, M. T. Asom, R. E. Leibenguth, G. D. Guth, and M. W. Focht. Appl. Phys. Lett. **63**, 2999–3001 (1993).

[11] K. D. Choquette, R. P. Schneider Jr., K. L. Lear, and R. E. Leibenguth. IEEE J. Selec. Top. Quantum Electron. **1**, 661–666 (1995).

[12] A. K. van Doorn, M. P. van Exter, and J. P. Woerdman. Appl. Phys. Lett. **69**, 1041–1043 (1996).

[13] D. V. Kuksenkov, H. Temkin, and S. Swirhun. Appl. Phys. Lett. **67**, 2141–2143 (1995).

[14] M. P. van Exter, M. B. Willemsen, and J. P. Woerdman. Phys. Rev. A **58**, 4191–4205 (1998).

[15] G. Giacomelli, F. Marin, M. Gabrysch, K. H. Gulden, and M. Moser. Opt. Commun. **146**, 136–140 (1998).

[16] K. D. Choquette, D. A. Richie, and R. E. Leibenguth. Appl. Phys. Lett. **64**, 2062–2064 (1994).

[17] J. Martín-Regalado, J. L. A. Chilla, J. J. Rocca, and P. Brusenbach. Appl. Phys. Lett. **70**, 3350–3352 (1997).

[18] K. Panajotov, B. Ryvkin, J. Danckaert, M. Peeters, H. Thienpont, and I. Veretennicoff. IEEE Photon. Technol. Lett. **10**, 6–8 (1998).

[19] R. F. M. Hendriks, M. P. van Exter, J. P. Woerdman, A. van Geelen, L. Weegels, K. H. Gulden, and M. Moser. Appl. Phys. Lett. **71**, 2599–2601 (1997).

[20] B. Ryvkin, K. Panajotov, A. Georgievski, J. Danckaert, M. Peeters, G. Verschaffelt, H. Thienpont, and I. Veretennicoff. J. Opt. Soc. Am. B **16**, 2106–2113 (1999).

[21] K. Panajotov, B. Nagler, G. Verschaffelt, A. Georgievski, H. Thienpont, J. Danckaert, and I. Veretennicoff. Appl. Phys. Lett. **77**(11), 1590–1592 (2000).

[22] M. San Miguel, Q. Feng, and J. V. Moloney. Phys. Rev. A **52**, 1728–1739 (1995).

[23] J. Martín-Regalado, F. Prati, M. San Miguel, and N. B. Abraham. IEEE J. Quantum Electron. **33**, 765–783 (1997).

[24] M. San Miguel. *Polarization properties of vertical cavity surface emitting lasers*. In A. Miller, M. Ebrahimzadeh, and D. M. Finlayson, editors, *Semiconductor quantum optoelectronics: From quantum physics to smart devices*, pages 339–366. SUSSP and Institute of Physics Publishing, Bristol (1999).

[25] C. H. Henry. IEEE J. Quantum Electron. **18**, 259–264 (1982).

[26] M. B. Willemsen, M. U. F. Khalid, M. P. van Exter, and J. P. Woerdman. Phys. Rev. Lett. **82**, 4815–4818 (1999).

[27] A. Valle, K. A. Shore, and L. Pesquera. Journal of Lightwave Technology **14**(9), 2062–2068 (1996).

[28] J. Martín-Regalado, S. Balle, M. San Miguel, A. Valle, and L. Pesquera. Quantum Semiclass. Opt. **9**, 713–736 (1997).

[29] G. Verschaffelt, J. Albert, B. Nagler, M. Peeters, J. Danckaert, S. Barbay, G. Giacomelli, and F. Marin. IEEE J. Quantum Electron. **39**, 1177–1186 (2003).

[30] B. S. Ryvkin and A.M. Georgievskiĭ. Semiconductors **33**(7), 813–819 (1999).

[31] A. K. van Doorn, M. P. van Exter, and J. P. Woerdman. IEEE J. Quantum Electron. **34**, 700–706 (1998).

[32] D. Burak, J. V. Moloney, and R. Binder. Phys. Rev. A **61**, 053809 (2000).

[33] A. K. van Doorn, M. P. van Exter, A. M. van der Lee, and J. P. Woerdman. Phys. Rev. A **55**, 1473–1484 (1997).

[34] M. Travagnin, M. P. van Exter, A. K. Jansen, A. K. J. van Doorn, and J. P. Woerdman. Phys. Rev. A **54**, 1647–1660 (1996).

[35] M. Travagnin. Phys. Rev. A **56**, 4094–4105 (1997).

[36] A. K. van Doorn, M. P. van Exter, and J. P. Woerdman. Appl. Phys. Lett. **69**, 3635–3637 (1996).

[37] M. Sondermann. *On polarization dynamics in vertical-cavity surface-emitting lasers: solitary devices and lasers with isotropic feedback.* Phd thesis, Westfälische-Wilhelms Universität Münster (2004).

[38] H. van der Lem and D. Lenstra. Opt. Lett. **22**, 1698–1700 (1997).

[39] H. F. Hofmann and O. Hess. Quantum Semiclass. Opt. **10**, 87–96 (1998).

[40] M. P. van Exter, A. Al-Remawi, and J. P. Woerdman. Phys. Rev. Lett. **80**, 4875–4878 (1998).

[41] J. Mulet, C. Mirasso, and M. San Miguel. Phys. Rev. A **64**, 023817 (2001).

[42] M. Sondermann, M. Weinkath, T. Ackemann, J. Mulet, and S. Balle. Phys. Rev. A **68**, 033822 (2003).

[43] R. A. Morgan, M. K. Hibbs-Brenner, T. M. Marta, R. A. Walterson, S. Bounnak, E. L. Kalweit, and J. A. Lehman. IEEE Photon. Technol. Lett. **7**, 441–443 (1995).

[44] M. Sondermann, M. Weinkath, and T. Ackemann. IEEE J. Quantum Electron. **40**, 97–104 (2004).

[45] C. Engler. *Polarisationsdynamik in oberflächen-emittierenden gewinngeführten Halbleiterlasern.* Diploma thesis, Westfälische Wilhelms-Universität Münster (2003).

[46] Yasuhiro Matsui, D. Vakhshoori, Peidong Wang, Peili Chen, Chih-Cheng Lu, Min Jiang, Kevin Knopp, Scott Burroughs, and Parviz Tayebati. IEEE J. Quantum Electron. **39**, 1037–1048 (2003).

[47] M. B. Willemsen, M. P. van Exter, and J. P. Woerdman. Phys. Rev. A **60**, 4105–4112 (1999).

[48] J.-L. Vey, C. Degen, K. Auen, and W. Elsäßer. Phys. Rev. A **60**, 3284–3295 (1999).

[49] Hitoshi Kawaguchi, I. S. Hidayat, Y. Takahashi, and Y. Yamayoshi. Electron. Lett. **31** (1995).

[50] Nancy Nieuborg, K. Panajotov, A. Goulet, I. Veretennicoff, and H. Thienpont. IEEE Photon. Technol. Lett. **10**, 973–975 (1998).

[51] T. Ackemann and M. Sondermann. Proc. SPIE **4286**, 44–54 (2001).

[52] P. Mandel and T. Erneux. Phil. Trans. R. Soc. Lond. A **313**, 285–290 (1984).

[53] F. Mitschke, R. Deserno, J. Mlynek, and W. Lange. Opt. Commun. **46**, 135–140 (1983).

[54] M. Sondermann. *Untersuchungen zum Polarisationsschalten in oberflächen-emittierenden Halbleiterlasern.* Diploma thesis, Westfälische Wilhelms-Universität Münster (2000).

[55] W. Lange, F. Mitschke, R. Deserno, and J. Mlynek. Phys. Rev. A **32**, 1271–1274 (1985).

[56] G. Giacomelli, F. Marin, and I. Rabbiosi. Phys. Rev. Lett. **82**, 675–678 (1999).

[57] B. Nagler, M. Peeters, J. Albert, G. Verschaffelt, K. Panajotov, H. Thienpont, I. Veretennicoff, J. Danckaert, S. Barbay, G. Giacomelli, and F. Marin. Phys. Rev. A **68**, 13813–1–8 (2003).

[58] M. B. Willemsen, M. P. van Exter, and J. P. Woerdman. Phys. Rev. Lett. **84**, 4337–4340 (2000).

[59] G. Verschaffelt, J. Albert, M. Peeters, K. Panajotov, J. Danckaert, I. Veretennicoff, H. Thienpont, F. Monti di Sopra, S. Eitel, R. Hoevel, M. Moser, H. P. Zappe, and K. Gulden. Proc. SPIE **3946**, 246–257 (2000).

[60] T. Ackemann and M. Sondermann. Appl. Phys. Lett. **78**, 3574–3576 (2001).

[61] M. Sondermann, T. Ackemann, J. Mulet, S. Balle, and K. Panajotov. Opt. Commun. **235**, 421–434 (2004).

[62] M. P. van Exter, R. F. M. Hendricks, and J. P. Woerdman. Phys. Rev. A **57**, 2080–2090 (1998).

[63] S. Balle, E. Tolkacheva, M. San Miguel, J. R. Tredicce, J. Martín-Regalado, and A. Gahl. Opt. Lett. **24**, 1121–1123 (1999).

[64] M. San Miguel, S. Balle, J. Mulet, C. Mirasso, E. Tolkachova, and J. R. Tredicce. Proc. SPIE **3944**, 242–251 (2000).

[65] G. Van der Sande, J. Danckaert, I. Veretennicoff, and T. Erneux. Phys. Rev. A **67**, 013809 (2003).

[66] M. Travagnin, M. P. van Exter, and J. P. Woerdman. Phys. Rev. A **56**, 1497–1507 (1997).

[67] S. Balle. Phys. Rev. A **57**, 1304–1312 (1998).

[68] W. van Haeringen. Phys. Rev. **158**, 256–272 (1967).

[69] D. Lenstra. Phys. Rep. **59**, 299–373 (1980).

[70] F. Prati, P. Caccia, and F. Castelli. Phys. Rev. A **66**, 063811 (2002).

[71] B. S. Ryvkin, E. A. Avrutin, and M. Pessa. J. Appl. Phys. **93**, 2353–2358 (2003).

[72] J. Danckaert, B. Nagler, J. Albert, K. Panajotov, I. Veretennicoff, and T. Erneux. Opt. Commun. **201**, 129–137 (2002).

[73] T. Erneux, J. Danckaert, K. Panajotov, and Veretennicoff. Phys. Rev. A **59**, 4660–4667 (1999).

[74] F. Prati, P. Caccia, M. Bache, and F. Castelli. Phys. Rev. A **69**, 033810 (2004).

[75] A. K. van Doorn, M. P. van Exter, M. Travagnin, and J. P. Woerdman. Opt. Commun. **133**, 252–258 (1997).

[76] E. L. Blansett, M. G. Raymer, G. Khitrova, H. M. Gibbs, D. K. Serkland, A. A. Allerman, and K. M. Geib. Opt. Express **9**(6), 312–318 (2001).

[77] P. Besnard, M. L. Charès, G. M. Stéphan, and F. Robert. J. Opt. Soc. Am. B **16**, 1059–1063 (1999).

[78] A. R. Cameron, P. Riblet, and A. Miller. Phys. Rev. Lett. **76**(25), 4793–4896 (1996).

[79] Y. Ohno, R. Terauchi, T. Adachi, F. Matsukura, and H. Ohno. Phys. Rev. Lett. **83**, 4196–4199 (1999).

[80] H. Ando, T. Sogowa, and H. Gotoh. Appl. Phys. Lett. **73**, 566–568 (1998).

[81] R. S. Britton, T. Grevatt, A. Malinowski, R. T. Harley, P. Perezzo, A. R. Cameron, and A. Miller. Appl. Phys. Lett. **73**, 2140–2142 (1998).

[82] C. J. Chang-Hasnain, J. P. Harbison, G. Hasnain, A. Von Lehmen, L. T. Florez, and N. G. Stoffel. IEEE J. Quantum Electron. **27**, 1402–1409 (1991).

[83] J. E. Epler, S. Gehrsitz, K. H. Gulden, M. Moser, H. C. Sigg, and H. E. Lehmann. Appl. Phys. Lett. **69**, 722–724 (1996).

[84] A. Barchanski, T. Gensty, C. Degen, I. Fischer, and Elsäßer W. IEEE J. Quantum Electron. **39**(7), 850–858 (2003).

[85] J. Mulet and S. Balle. IEEE J. Quantum Electron. **38**(3), 291–305 (2002).

[86] J. Mulet and S. Balle. Phys. Rev. A **66**, 053802 (2002).

[87] S.P. Hegarty, G. Huyet, J. G. McInerney, and K. D. Choquette. Phys. Rev. Lett. **82**, 1434–1437 (1999).

[88] N. A. Loiko and I. V. Babushkin. J. Opt. B: Quantum Semiclass. Opt. **3**, S234–S243 (2001).

[89] T. Rössler, J. V. Moloney, and T. Ackemann (2003). Submitted to Phys. Rev. A.

[90] Y. F. Chen, K. F. Huang, H. C. Lai, and Y. P. Lan. Phys. Rev. Lett. **90**, 053904 (2003).